Chapter 1

Bunch length measurement

The length of a particle bunch is rather difficult to measure at lepton accelerators where this length is typically less than a millimeter, corresponding to bunch durations much shorter than what can be measured by fast detectors [1]. It is therefore necessary to convert the bunch length into another quantity that can be measured. Coherence is both a motivation and a tool to measure such length. Coherent collective effects such as coherent synchrotron radiation can significantly disrupt a beam. Their dependance on the beam current and not the beam charge means that to control them it is necessary to measure the bunch length instead of simply the bunch charge. As a counterpart, coherent radiation is one of the means of measuring a bunch length.

In plasma acceleration with external injection (such as FACET's E-200 [1], AWAKE [2] or ESCULAP [3]) this bunch length measurement is important to estimate which fraction of the bunch will fit in the acceleration buckets created in the plasma. As with the transverse measurements, at a plasma accelerator it is necessary to make the measurement in a single shot for it to be meaningful.

When the resolution is sufficient the bunch length measurement can become a bunch profile measurement as is the case with the methods based on coherent radiation methods.

I have worked on one of these techniques using Coherent Smith-Purcell Radiation for several years.

[1] Because in lepton accelerators the particles travel at the speed of light there is a direct correlation between bunch length and bunch duration. It results that abusingly the bunch length is often quoted with time units. A bunch duration of 1 ps corresponds to a bunch length of 0.3 mm

1.1 Bunch length and bunch profile measurement techniques

Several other techniques allow for bunch length measurements and I will first review them.

1.1.1 Techniques based on current transformers

Bunch charge can be measured using current transformers (CT). Depending on the application, there are several flavors of current transformers : AC-Current Transformers (ACCT), DC-Current Transformers (DCCT), Integrating Current Transformers (ICT), ... They all measure the current induced by the beam in a gap of the beam pipe to estimate the beam current. Depending on the signal amplification required the measurement device can be a simple wire connected to an ammeter or a coil with several windings connected to an ammeter or to more complicated electronics. The working principle and an example of current transformer are shown on figure 1.1.

When the time resolution of the current measuring device is good enough and the impedance low enough the current transformer can give information about the variation of the current with them and therefore the bunch length, however this is true only for beams that are at least several centimeters long (nanosecond duration).

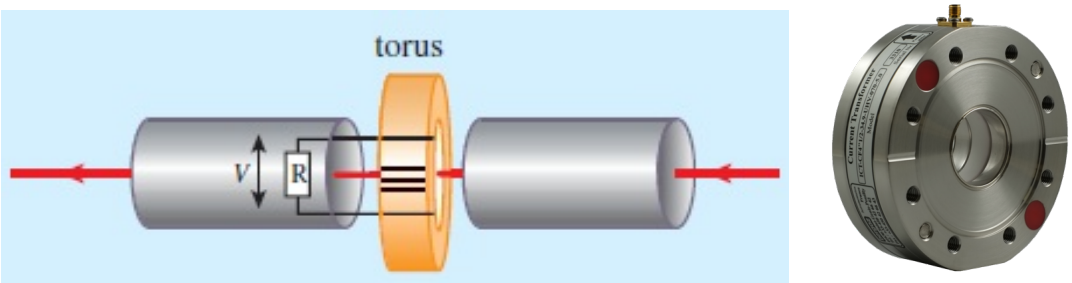

Figure 1.1: (Left) Principle of a current transformer used for beam charge measurement : when the particle beam passes through a torus it induces a current proportional to the beam charge in the torus coil windings, allowing for beam charge measurement. (Right) Example of current transformer as sold by a well-known manufacturer [4].

1.1.2 Techniques based on longitudinal to transverse exchange

For beam with a length in the millimeter range (or below) it is more difficult to measure their length or their profile in the longitudinal direction (that is the direction of propagation) than their transverse properties. Exchanging the longitudinal direction with one of the transverse directions can therefore make this measurement easier.

A **Streak Camera** is a device available commercially that can achieve this fate : in a streak a photon beam hits a photocathode and is converted by photoemission in a low energy (keV) electron beam. This electron beam passes between two electrodes to which are applied a high frequency high voltage electric field that will streak the electron beam transversely, the electron deflection being proportional to their arrival time. After the electrodes the electron beam hit a luminescent screen where the transverse profile of the electrons after streaking can be observed. Thus it is possible to obtain the longitudinal profile of the photon beam (convoluted with one of its transverse profile). Commercial streak camera can reach a resolution of about 1 ps on photon beams.

A **Streak Camera combined with a radiation emitting screen**, such as a sapphire screen emitting Cerenkov radiation can be used to image the longitudinal profile of an electron beam with MeV energy or higher. Such method was tested for example at the CANDELA photo injector at LAL [5]. However this method is limited by the spread in the longitudinal profile induced by the screen itself and by the photon beam transport (usually to the outside of the accelerator) and therefore it is not available to measure sub-picoseconds beams.

Streak camera are often used in rings to measure the bunch length using the synchrotron radiation emitted[6, 7].

This can be mitigated by deflecting directly the high energy electrons using a **deflecting RF cavity**. This requires the electric field to be high enough to deflect high energy electrons and to have a high enough frequency to streak significantly the beam. The state of the art in this field has been demonstrated at SLAC recently on both LCLS and FACET accelerators [8], reaching resolutions of 10 fs at 14 GeV and SI70fs at 20 GeV. However the cost of such device, including the associated RF power source is more than a million euros.

A cheaper solution to streak the electrons is to use the so-called **3-phases method** [9, 10] in which one of the accelerating section of the accelerator is dephased to provide a longitudinal streaking effect that can be measured as a variation in the beam energy dispersion. This method has the advantage of being much cheaper but is limited in its resolution by the power of the accelerating cavity and the resolution of the dispersion measurement setup. A resolution of a few picoseconds has been demonstrated experimentally.

1.1.3 Measures based on radiation emitted by the beam

Instead of manipulating the beam to measure it, it is possible to measure the radiation it emits and use it to get information on its longitudinal profile. This is what is done with the streak camera based measurements described above but other methods rely on this technique.

In the **electro-optic sampling** method a birefringent crystal is brought close from the

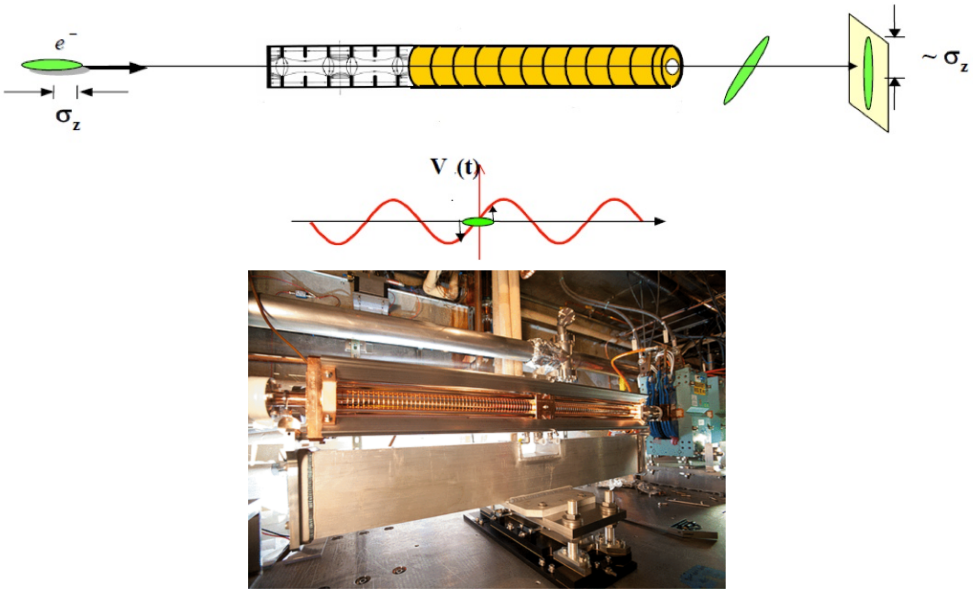

Figure 1.2: Left: The principle of the Transverse deflecting cavity used at SLAC to measure bunches longitudinal profiles (Image taken from https://portal.slac.stanford.edu/sites/ard_public/facet/facilities/Pages/TCAV.aspx). Right: A photo of the FACET transverse deflecting cavity (image taken from [8]).

electron beam and a chirped ultrafast laser pulse[2] is shone on it. The electromagnetic field of the electron beam will induce a change in the refraction index of the crystal in at least one of the polarisation plane. As the laser pulse is chirped a diffraction grating can then be used to measure its longitudinal profile projected on a screen. Thus by comparing the longitudinal profile of the two polarisation components it is possible to deduce the changes that occurred in the crystal as fonction of time and therefore the bunch longitudinal profile. This is a well known technique in optics (for example to measure and profile THz pulses) that has been applied to accelerators by several groups (including, for example, [11, 12, 13]). This technique is illustrated on figure 1.3.

The electromagnetic spectrum emitted by the electron bunch is modulated by the bunch length: when a photon is emitted in an electron bunch, if the wavelength of that photon is larger than the separation between two photons, then the two photons will contribute and the emission probability is increased. When N photons contribute the probability increases as $N(N-1)$.

It is possible to define the "form factor" ($\mathcal{F}$) of the radiation emitted by an electron bunch as:

[2]This means that the photons of the laser pulse have a correlation between wavelength and longitudinal position. This is a common techniques with lasers and can be done, for example, by using a set of diffraction gratings.

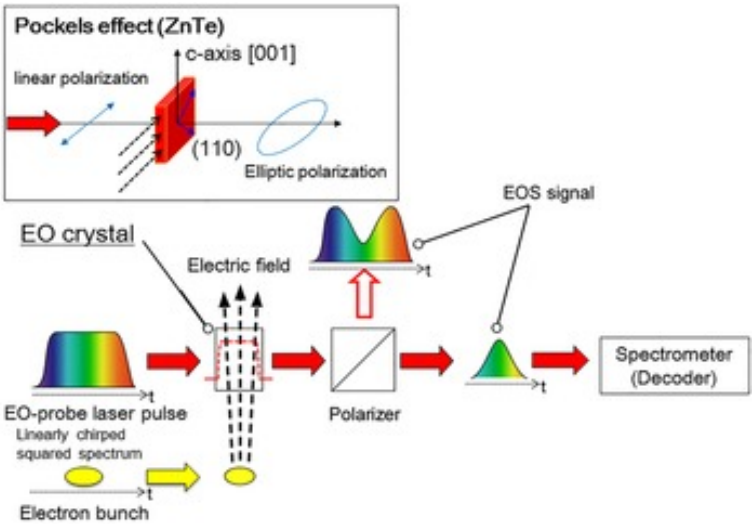

Figure 1.3: Principle of bunch length measurements using electro-optic sampling (taken from [13]

$$\mathcal{F}(\nu) = \left|\int_{-\infty}^{+\infty} S(x)\exp\left(i\frac{2\pi\nu}{c}x\right)dx\right| \times \left|\int_{-\infty}^{+\infty} S(y)\exp\left(i\frac{2\pi\nu}{c}y\right)dy\right| \times \left|\int_{-\infty}^{+\infty} S(z)\exp\left(i\frac{2\pi\nu}{c}z\right)dz\right| \tag{1.1}$$

where ν is the photons' frequency, $S(x)$, $S(y)$ and $S(z)$ are the profile distribution along x, y and z respectively. And the total radiation intensity I_{tot} emitted for a given radiative phenomena at a given frequency will be:

$$I_{tot}(\nu) = I_1(\nu)\left(N + N(N-1)\mathcal{F}(\nu)\right) \tag{1.2}$$

where I_1 is the single electron yield for the phenomena and N the number of electrons. This radiation can be used in several different manners to measure the bunch length and its longitudinal profile.

Coherent Transition Radiation (CTR) is emitted when a bunch of charged particles passes through a thin foil. Several groups [14, 15, 16] have studied how to measure the spectrum of the CTR emitted and used it to reconstruct bunch length. The SLAC group [14] uses a KRS-5 prism to disperse the infrared radiation collected and focus it on a detector. The Frascati group [15] uses a Martin-Puplett interferometer to study the THz radiation produced by their CTR screens. These setups are shown on figure 1.4. It should be noted that the methods used by these two groups require a scan of the dispersive element or of the interferometer to measure the radiation spectrum. To overcome this difficulty the DESY group [16] uses several dispersive gratings with several detectors to perform this measurement (see figure 1.5).

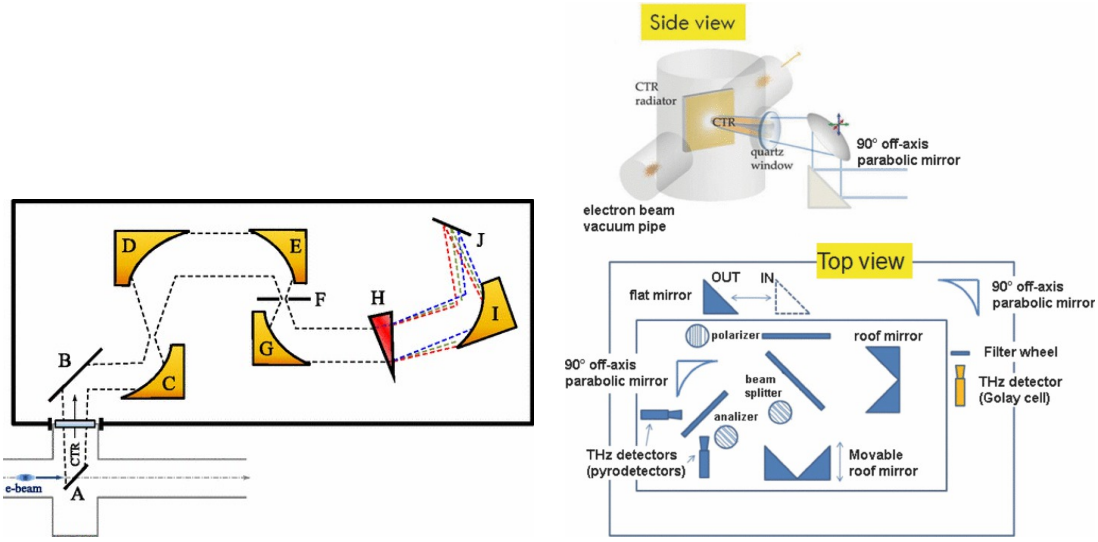

Figure 1.4: Principle of Coherent Transition Radiation measurements at SLAC on LCLS and FACET (left; taken from [14]) and at SPARC (right taken from [15]).

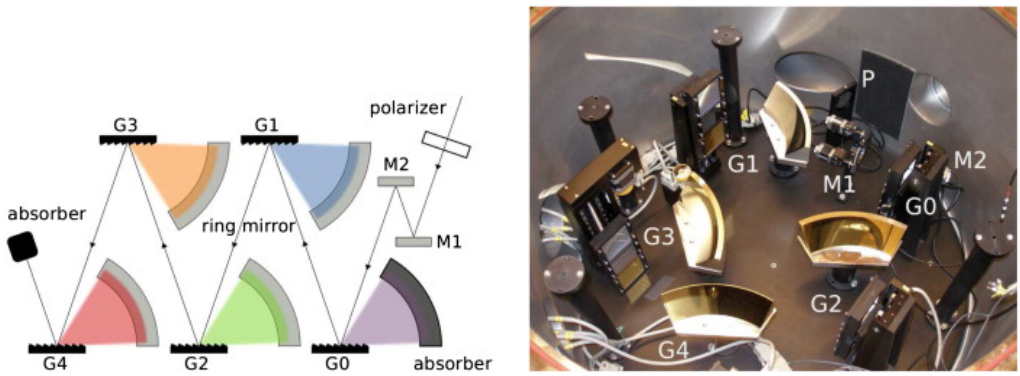

Figure 1.5: Principle XX of the Coherent Transition Radiation single shot setup at DESY (schematic and picture).

The SLAC group has published their ability to reconstruct 3 fs to 60 fs-long bunches.

Another way to measure the radiation emitted by the bunch is to measure the **Coherent Smith-Purcell Radiation (CSPR)** it emits. CSPR is emitted when a metallic diffraction grating is brought close from the beam. I have worked extensively on CSPR for several years and it is described details in section 1.2.

1.1.4 Comparison of longitudinal bunch measurement techniques

The different longitudinal bunch measurement techniques are summarized in tables 1.1 and 1.2.

From theses tables it appears that there is a wide range of cost and complexity among longitudinal bunch length measurements. The use of RF deflecting cavities is both complex and expensive (the price been dependent on the beam energy and the RF band chosen for the measurement) but it is used at several accelerators as a reference to measure the bunch length [3]. This has triggered research to find cheaper techniques. Electro-optic sampling is a technique that was already available from the optics community, however it is complex as it requires an ultrafast laser that is hardly compatible with an accelerator enclosure and therefore requires to transport the ultrashort laser pulses inside the accelerator enclosure. CTR has the advantage of being even cheaper and less complicated to setup and several groups have investigated it and solved differently the problem of spectrum measurement. CSPR is a less known phenomena and therefore it has been investigated by fewer groups but renewed interest appeared because of its single shot and non-destructive capability.

The interest for Energy Recovery Linac (ERL) may also increase the need for non destructive single shot longitudinal diagnostics: current ERLs have shown that correct operations require a very good understanding of the bunch longitudinal phase space at different locations along the ERL. The availability of a non destructive fast diagnostics would therefore be an advantage for such machine and in particular for the machine that is planned to be built in Orsay.

[3] A comparison of Electro-optic sampling, streak cameras and RF deflecting cavities as longitudinal bunch profile diagnostic for FACET has been published in [17].

Name	Main technology	Best resolution	Cost	Availability status
Current transformer	Coil	Limited by electronics $\mathcal{O}$ 100 ps	$\mathcal{O}$ 10k€	Commercially available Commonly used
Streak camera with radiator	Photocathode, High Voltage	Limited by high voltage frequency $\mathcal{O}$ ps	$\mathcal{O}$ 300k€	Camera commercially available Setup: R&D
RF deflector	High power RF + cavity C-band or X-band RF	$\mathcal{O}$ 10 fs	$\mathcal{O}$ 500k€- 2M€ (energy dependent)	R&D product distributed by one manufacturer
3 phases	RF cavities	$\mathcal{O}$ ps	Use linac infrastructure	Commonly used
Electro-optic sampling	Laser Birefringent crystals	$\mathcal{O}$ 50 fs (better res. in optics)	Laser: $\mathcal{O}$ 200k€ Other: $\mathcal{O}$ 50k€	Commonly used in optics
Coherent Transition Radiation	Optics THz filtering	$\mathcal{O}$ 10 fs	$\mathcal{O}$ 50k€	In use at several facilities
Coherent Smith-Purcell Radiation	Diff. gratings THz filtering	$\mathcal{O}$ 50 fs	$\mathcal{O}$ 50k€	R&D

Table 1.1: Comparaison of the properties of the different techniques of longitudinal bunch length and profile measurement

Name	Single shot capability	Beam destruction
Current transformer	Yes	No
Streak camera with radiator	Yes	Radiator dependent Synchrotron radiation: No; Screen: Yes
RF deflector	Partially The phase of the measurement must be checked	Yes
3 phases	No	Yes (beam off-energy)
Electro-optic sampling	Yes	No
Coherent Transition Radiation	Interferometer: No Multpl. Gratings: Yes	Yes
Coherent Smith-Purcell Radiation	Yes	No

Table 1.2: Comparaison of the capabilities of the different techniques of longitudinal bunch length and profile measurement

1.2 Smith-Purcell Radiation

1.2.1 First observation of Smith-Purcell Radiation

The first observation of what is now called Smith-Purcell Radiation dates back to 1953 when Smith and Purcell reported the observation of visible light from localized surface charges moving across a grating [18]. Their observation was made using 300 keV electrons in a continuous beam. An image of this observation is shown on figure 1.6.

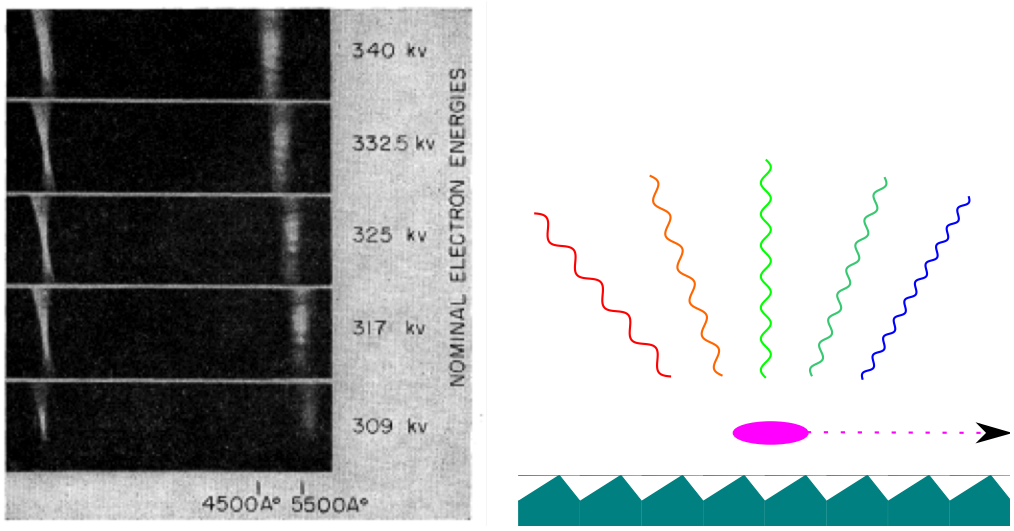

Figure 1.6: Left: Image taken from [18] showing the observation of radiation by Smith and Purcell in 1953. Right: Schematic of Smith-Purcell radiation.

The first observation of Smith-Purcell radiation from relativistic electrons was reported only much later in 1992 [19] and the first observation of Coherent Smith-Purcell Radiation [20] came in 1995.

XXX coherent / relativistic images

XXX Van den berg P. M. van den Berg, J. Opt. Soc. Am. 63, 1588 1973!.

1.2.2 Interpretation of Smith-Purcell Radiation

The phenomena was further studied and several interpretations were proposed:

- According to Ishiguro and Tako's interpretation [21], Smith-Purcell radiation comes from dipole radiation: when an electron beam passes above a grating it induces a current in the grating; the oscillations of this current in the teeth of the grating will create dipole radiation that is emitted. This will later be referred to as the "surface current" interpretation. This interpretation is shown on figure 1.7 (left).

- Toraldo di Francia proposed a different interpretation [22]: according to him a charged particle in straight uniform motion generates a field that can be expanded into a set of evanescent waves. It is the diffraction of these waves on a diffraction grating that creates the Smith-Purcell radiation. This will later be referred to as the "radiation diffraction" interpretation. This interpretation is shown on figure 1.7 (right).

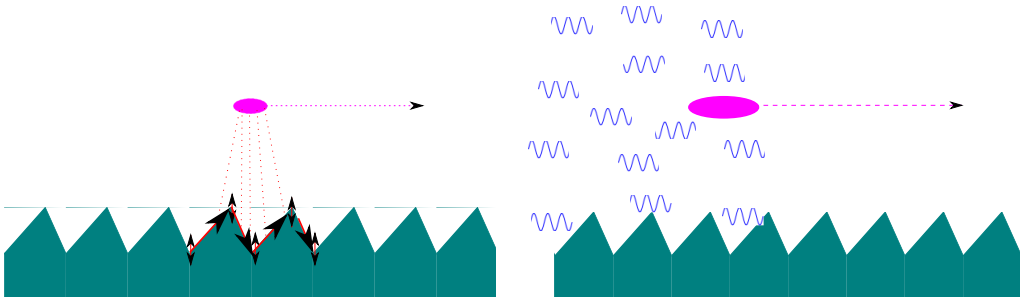

Figure 1.7: The two interpretation of Smith-Purcell radiation: The surface current interpretation as in [21] (left) and the radiation diffraction interpretation as in [22] (right).

Although these interpretations are different, the underlying physics is the same and the interpretations should yield to comparable predictions. A comparison of several Smith-Purcell radiation models has been published in [23] and based on that paper I worked with a student to perform such comparison for parameters relevants to the experiments we were conducting [24]. Our conclusion was that within an order of magnitude all models have to comparable single electron yield as shown on figure 1.8.

1.2.3 Application of Smith-Purcell Radiation

Smith-Purcell radiation and later CSPR have been seen by many scholars as a potential source of high power infrared radiation, leading for example to a patent to that purpose [27]. As early as 1979, Smith-Purcell radiation has also been seen by some scholars as a promising tool to seed Free Electron Lasers [28, 29, 30, 31, 32] and has been patented [33].

The use of CSPR as a bunch longitudinal profile diagnostic was proposed soon after the first observation of CSPR and it was even patented [34] (for the US only) at that time. More detailed work was published by a different team in 2002 [35, 36] and several key steps were done in the following years [37, 38], including in teams in which I was participating [39, 40, 41, 42].

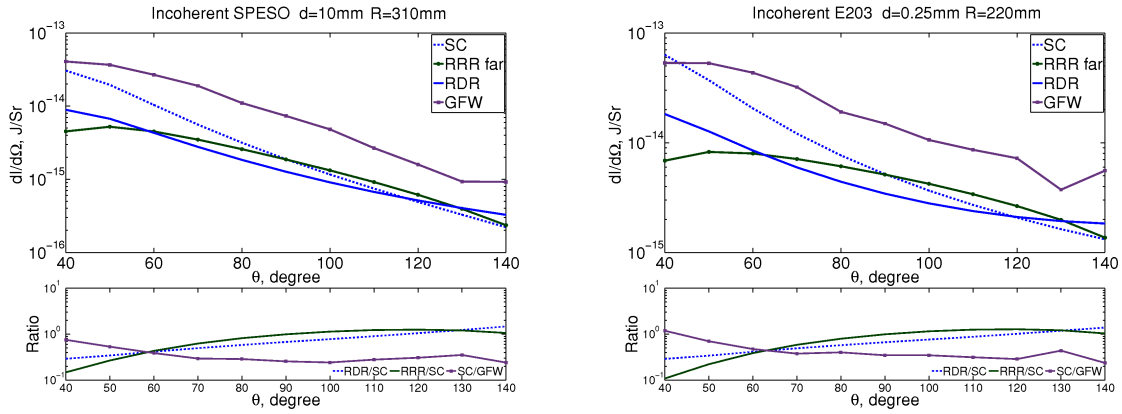

Figure 1.8: Comparison of the single electron yield of different Smith-Purcell Radiation models (as published in [24]): the solid blue line corresponds to the Resonant Diffraction Radiation (RDR) model [23], the green line to the Resonant Reflection Radiation (RRR) model [25], the purple line with square marker label GFW to the Surface Current model as described in [26] and the blue dashed line also to the Surface Current (SC) model described in [26] but with the grating coupling efficiency expression taken from [23]. See [24] for details.

1.2.4 Theoretical aspects of Smith-Purcell Radiation

The theory of Smith-Purcell radiation has been developed in several publications. The most relevant of them, based on the surface current model, being [26, 43]. The discussion below is based on these articles.

A diffraction grating will reflect light in different directions by interferences between the rays reflected by each surface. As shown on figure 1.10, reflections corresponding to the simple Snell-Descartes law are called "Order 0". Higher order correspond to interferences between all the teeth (order 1) or part of the teeth.

The coordinate system used in this chapter is shown on figure 1.9.

The relation between the polar angle of observation θ (in the plane perpendicular to the grating surface and passing by the beam), the grating pitch l and the wavelength λ of the emitted radiation is given by

$$\lambda = \frac{l}{n}\left(\frac{1}{\beta} - \cos\theta\right) \tag{1.3}$$

where n is the radiation order and $\beta = \frac{v}{c}$ is the ratio between the particle speed v and the speed of light c. In lepton accelerator it is often very close to 1. This relation is purely a consequence of the fact that waves emitted by a grating will interfere and in each direction constructive interferences correspond to specific wavelengths.

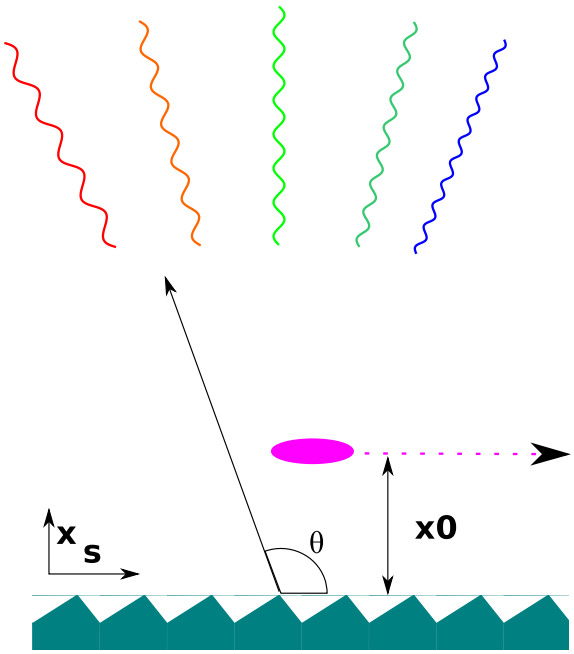

Figure 1.9: Coordinates system used in this chapter. The direction z comes out of the figure plane as is the azimuthal angle ϕ.

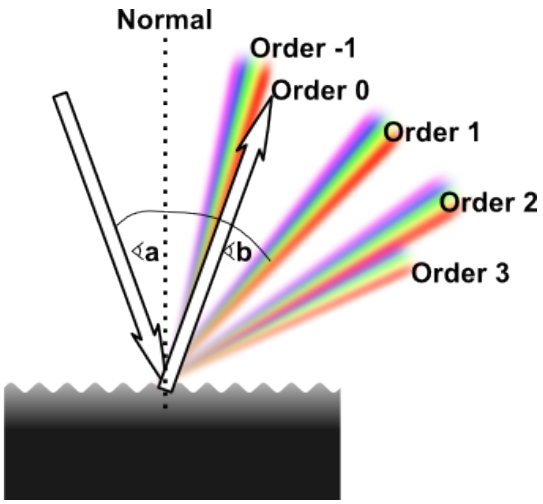

Figure 1.10: The different orders of a grating: order 0 corresponds to a simple reflection, the other orders corresponds to interferences of the wavelengths reflections. Image taken from [44].

The intensity of radiation emitted by a single electron (single electron yield), per unit solid angle (Ω) and per frequency (ω) is given by

$$\frac{d^2I_1}{d\omega d\Omega} = \frac{e^2\omega^2 l^2}{4\pi^2 c^3} R^2 \exp\frac{-2x_0}{\lambda_e} \tag{1.4}$$

where e is the electron charge, x_0 is the beam grating separation, λ_e is the evanescent wavelength of the virtual radiation emitted by the beam and R^2 is a factor reflecting the coupling of the beam with the grating.

The evanescent wavelength is given by

$$\lambda_e = \lambda \frac{\beta\gamma}{2\pi\sqrt{1+(\beta\gamma\sin\theta\sin\phi)?2}} \tag{1.5}$$

where γ is the Lorentz factor, ϕ is the azimuthal angle (the ascension above or below the plane perpendicular to the grating surface and passing by the beam).

As discussed above, equation 1.2 applies to Smith-Purcell Radiation and the total radiation intensity emitted from a charged particle bunch of multiplicity N is given by:

$$\frac{d^2I}{d\omega d\Omega} = \frac{d^2I_1}{d\omega d\Omega}\left[N + N(N-1)\mathcal{F}(\omega)\right] \tag{1.6}$$

where $\mathcal{F}(\omega)$ is the form factor introduced in equation 1.1.

One important difference between CSPR and other radiative methods is that the choice of the grating will change the radiation intensity observed at different frequencies. On figure 1.11 one can see the radiation intensities observed for the same bunch profile but with different gratings pitches.

Improving the beam-coupling calculation

The factor R^2 is rather complicated to estimate. It has been discussed in details in [45] and an approximate solution has been given for high energy beams in the case of echelette gratings.

The equation 1.3 is very similar the the standard grating equation in the Littrow condition (with the same definition of variables as above) [46]:

$$\lambda = \frac{2l\sin\theta}{n} \tag{1.7}$$

This has led me to study with a student [**?**] whether it would be possible to benefit from the advanced work done in the field of grating theory [47] to estimate R^2. We produced some predictions but these are rather close to what has been obtained with

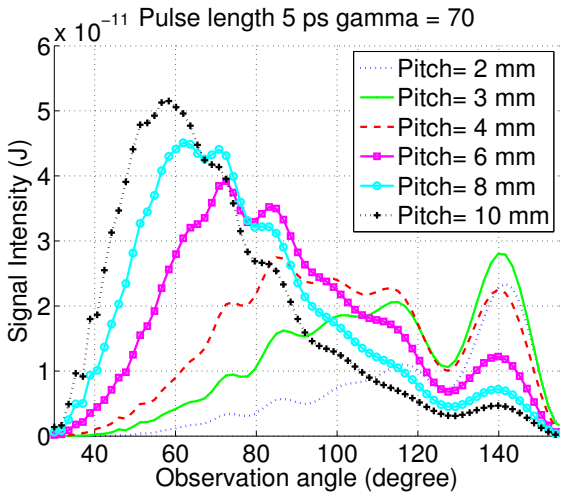

Figure 1.11: Radiation profiles observed for the same pulse but for different grating pitches.

simulation codes based on [45] and therefore we have not yet been able to distinguish the two approaches. This may become possible at the experiment described in 1.3.3.

It should be noted that with the advent of fast and powerful Particle-in-cell electromagnetic simulation softwares, it becomes possible to simulate the electromagnetic effects that a charged particles beam induces near a grating without relying on the models described above. This is what has been attempted in [**?**].

1.2.5 Profile recovery

As we can see in equation 1.6, there is a mathematical relation between the form factor and the CSPR intensity at each wavelength. Using relation 1.3 we see that this means that the signal intensity measured at different angles depends on the form factor and therefore encodes the bunch length. Calculating the form factor from the measured signal is therefore rather straightforward.

We have also seen in equation 1.1 that the form factor is strongly related to the bunch longitudinal profile. However the inverse operation is not so easy: some information is lost due to the absolute values in equation 1.1. The knowledge of the form factor alone requires more complicated mathematics to recover the profile.

The Fourier transform of a physical function satisfies the Cauchy-Riemann equations therefore a given real function (the measured form factor) can only be matched to a very limited number of imaginary functions and usually by adding extra conditions there will be only one remaining acceptable imaginary (phase) function. This phase function can be found using a Hilbert transform or the Kramers Kronig (KK) relations.

To recover the phase of a form factor, it must first be written in the following form:

$$log(\mathcal{F}(\omega)) = log(\rho(\omega)) + i\Theta(\omega) \tag{1.8}$$

where $\rho(\omega))$ is the amplitude and $\Theta(\omega)$ the phase associated to this Form factor. $\rho(\omega))$ is thus the result of the measurement and $\Theta(\omega)$ the information that needs to be recovered.

The Hilbert transform gives then the relation

$$\Theta(\omega_0) = -\frac{1}{\pi} P \int_{-\infty}^{+\infty} \frac{ln(\rho(\omega))}{\omega_0 - \omega} d\omega. \tag{1.9}$$

and the Kramers Kronig relation gives:

$$\Theta(\omega_0) = \frac{2\omega_0}{\pi} P \int_{0}^{+\infty} \frac{ln(\rho(\omega))}{\omega_0^2 - \omega^2} d\omega \tag{1.10}$$

In most cases the value given by these two methods will be very close.

Before I started working on CSPR an algorithm based on KK was already available [**?**] for all coherent radiation phenomena. However its implementation for CSPR was sometimes leading to non-sensical results. With a student (Vitalii Khodnevych), we implemented and studied a new phase recovery algorithm based on the Hilbert transform [**?**]. We extended this work by doing a large number of simulations to also study the precision of this algorithm, how to optimise the position and number of detectors and how noise can affect the quality of the measurement [**?**]. The main results of this paper are presented below.

To study how profiles shapes match each other we defined a variable by analogy to the standard Full-Width at Half-Maximum (FWHM), this variable called Full-Width at X of the Maximum (FWXM) allows to study the width of a pulse at a certain fraction X of the maximum. The FW0.5M is similar to the usual FWHM. To compare the shape of a reconstructed profile (deco) and its orignal (orig) we define the variable Δ_{FWXM} as follow:

$$\Delta_{FWXM} = \left| \frac{FWXM_{\text{orig}} - FWXM_{\text{reco}}}{FWXM_{\text{orig}}} \right| \tag{1.11}$$

Figure 1.12 for example shows example of simulated profiles correctly reconstructed but also profiles poorly reconstructed. Figure 1.13 studies the impact of the number of detectors of the quality of the reconstruction, showing that there is an optimum at about 3×11 detectors (3 sets of 11 detectors covering different frequency ranges) and figure 1.14 shows that positioning them at constant angle is better than positioning them linearly or logarithmically (in frequency), examples of possible detectors positioning are

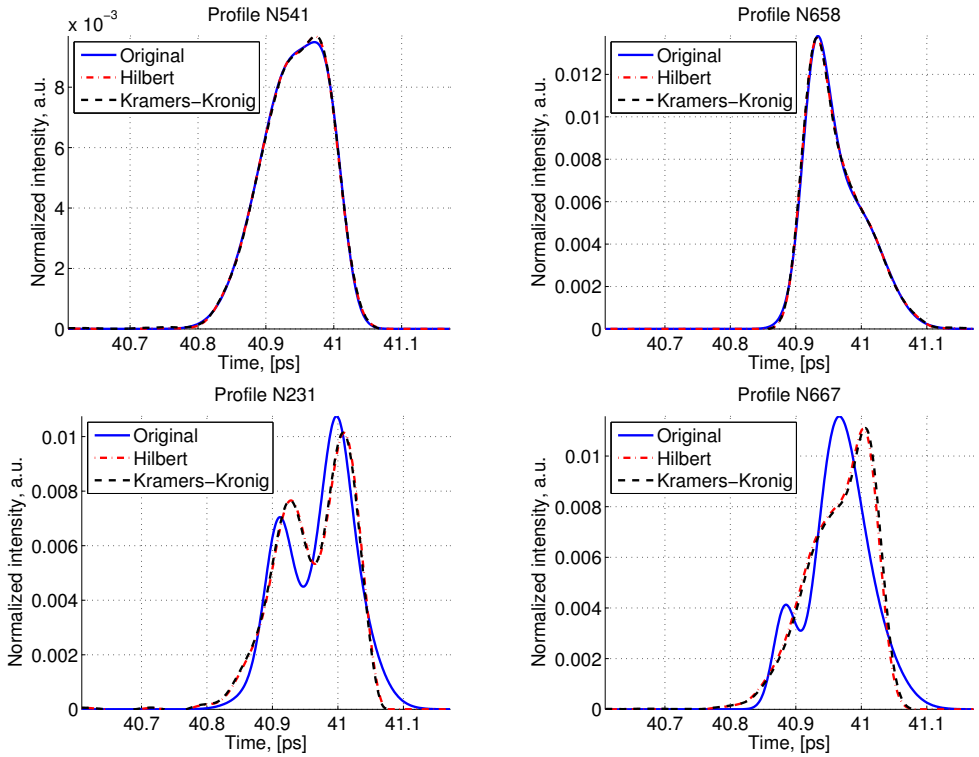

Figure 1.12: Example of profiles correctly reconstructed (upper row) and poorly reconstructed (lower row) as presented in [**?**]. The original profile is in blue and the profiles reconstructed with the Hilbert transform and the full Kramers-Kronig procedures are in red and black respectively.

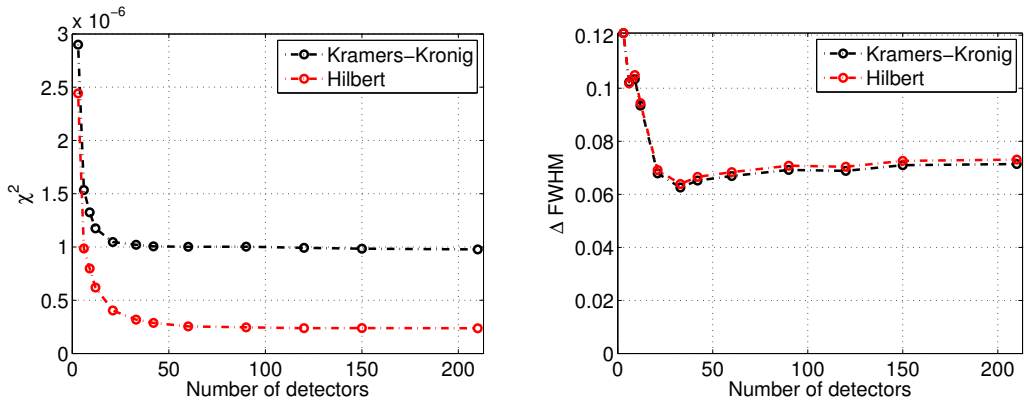

Figure 1.13: Effect of the sampling frequencies (number of detectors) on the χ^2 (left) and Δ_{FWHM} (right) when comparing original an reconstructed profiles, as presented in [**?**].

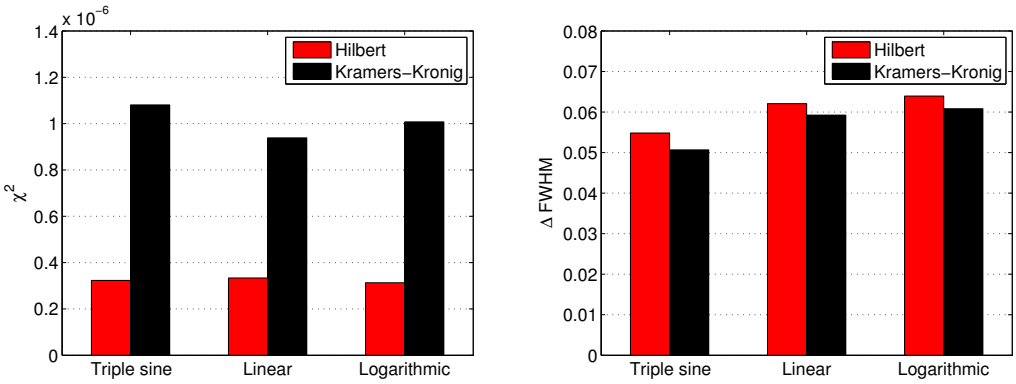

Figure 1.14: Comparison of different samplings methods using the χ^2 criterion (left) and Δ_{FWHM} (right), as presented in [**?**].

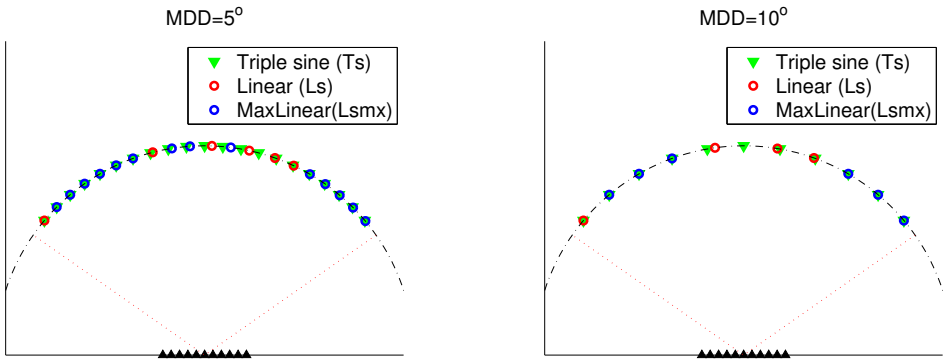

Figure 1.15: Examples of detector positions for different types of sampling for a minimal detector distance of 5^o (left) and 10^o (right), as presented in [**?**] .

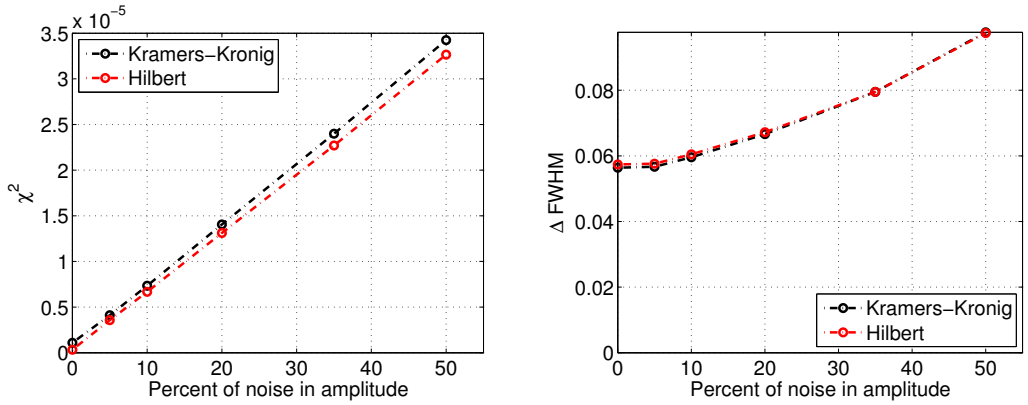

Figure 1.16: Mean χ^2 and Δ_{FWXM} as function of the noise amplitude, as presented in [**?**]. The interpretation of this figure is that with a 50% noise on our signal we introduce an error on the profile FWHM of about 10%.

shown on figure 1.15. Finally we also studied the effect of noise on the measured signal on the quality of the reconstruction 1.16.

Image CLIO 3 diff profiles

1.3 Experimental study of Coherent Smith-Purcell radiation

One of the remaining difficulties preventing the adoption of Smith-Purcell radiation as a longitudinal profile is that

1.3.1 Smith-Purcell radiation measurement at FACET

1.3.2 Smith-Purcell radiation measurement at SOLEIL

1.3.3 Smith-Purcell radiation measurement at CLIO

.

1.3.4 Outlook: Application to laser-driven plasma accelerators and ERLs

beam grating sep. stability

1.4 Undefined references

chap:plasmaAccelerationMecanism chap:laser-wire chap:pepper-pot chap:SP laser-synch chap:laser-plasma

Bibliography

[1] M. Litos, E. Adli, W. An, C. I. Clarke, C. E. Clayton, S. Corde, J. P. Delahaye, R. J. England, A. S. Fisher, J. Frederico, S. Gessner, S. Z. Green, M. J. Hogan, C. Joshi, W. Lu, K. A. Marsh, W. B. Mori, P. Muggli, N. Vafaei-Najafabadi, D. Walz, G. White, Z. Wu, V. Yakimenko, and G. Yocky. High-efficiency acceleration of an electron beam in a plasma wakefield accelerator. *Nature*, 515(7525):92–95, 11 2014.

[2] Allen Caldwell, Konstantin Lotov, Alexander Pukhov, and Frank Simon. Proton-driven plasma-wakefield acceleration. *Nat Phys*, 5(5):363–367, 05 2009.

[3] Nicolas Delerue, Christelle Bruni, Stéphane Jenzer, Sophie Kazamias, Bruno Lucas, Gilles Maynard, and Moana Pittman. Simulations of the Acceleration of Externally Injected Electrons in a Plasma Excited in the Linear Regime. In *arXiv 1607.02065 - IPAC'16, WEPMY0003*, 2016.

[4] Bergoz http://www.bergoz.com/ict-bcm-ihr.

[5] G. Devanz, B. Leblond, B. Mouton, and C. Travier. Bunch length measurement on CANDELA photoinjector. *Conf. Proc.*, C9608262:761–763, 1996.

[6] C. M. Thomas and G. Rehm. Diamond optical diagnostics: First streak camera measurements. *Conf. Proc.*, C060626:1112–1114, 2006. [,1112(2006)].

[7] M.-E. Couprie R. Nagaoka D. Pedeau M. Labat, L. Cassinari. Streak camera measurements of the soleil bunch length. In *Proceedings, DIPAC 2007*, page wepb05, 2007.

[8] Valery A. Dolgashev, Gordon Bowden, Yuantao Ding, Paul Emma, Patrick Krejcik, James Lewandowski, Cecile Limborg, Michael Litos, Juwen Wang, and Dao Xiang. Design and application of multimegawatt x-band deflectors for femtosecond electron beam diagnostics. *Phys. Rev. ST Accel. Beams*, 17:102801, Oct 2014.

[9] F. Glotin, J.-M. Berset, R. Chaput, D. A. Jaroszynski, J.-M. Ortéga, and R. Prazérès. Bunch length measurements on CLIO. *Nuclear Instruments and Methods in Physics Research A*, 341:49–53, March 1994.

[10] Thomas Vinatier, Christelle Bruni, Sophie Chancé, and Patrick Puzo. Length Measurement of High-brightness Electron Beam thanks to the 3-Phase Method. In *Proceedings, 5th International Particle Accelerator Conference (IPAC 2014): Dresden, Germany, June 15-20, 2014*, page THPME095, 2014.

[11] X. Yan, A. M. MacLeod, W. A. Gillespie, G. M. H. Knippels, D. Oepts, A. F. G. van der Meer, and W. Seidel. Subpicosecond electro-optic measurement of relativistic electron pulses. *Phys. Rev. Lett.*, 85:3404–3407, Oct 2000.

[12] Y Parc, Changbum Kim, Jung Yun Huang, Jangho Park, Taiha Joo, and In Soo Ko. A study of electro-optical crystal as a diagnostic tool for low energy electron beam. *JOURNAL-KOREAN PHYSICAL SOCIETY*, 50(5):1390, 2007.

[13] H. Tomizawa, T. Sato, K. Ogawa, K. Togawa, T. Tanaka, T. Hara, M. Yabashi, H. Tanaka, T. Ishikawa, T. Togashi, and et al. Stabilization of a high-order harmonic generation seeded extreme ultraviolet free electron laser by time-synchronization control with electro-optic sampling. *High Power Laser Science and Engineering*, 3, 2015.

[14] T. J Maxwell, C. Beherens, Y. Ding, A. S. Fisher, J. Frisch, Z. Huang, and H. Loos. Coherent Radiation Spectroscopy of Few-Femtosecond Electron Bunches Using a Middle-Infrared Prism Spectrometer. *Phys. Rev. Lett.*, 111(18):184801, 2013.

[15] E. Chiadroni, M. Bellaveglia, P. Calvani, M. Castellano, L. Catani, A. Cianchi, G. Di Pirro, M. Ferrario, G. Gatti, O. Limaj, S. Lupi, B. Marchetti, A. Mostacci, E. Pace, L. Palumbo, C. Ronsivalle, R. Pompili, and C. Vaccarezza. Characterization of the thz radiation source at the frascati linear accelerator. *Review of Scientific Instruments*, 84(2):022703, 2013.

[16] Stephan Wesch, Bernhard Schmidt, Christopher Behrens, Hossein Delsim-Hashemi, and Peter Schmuser. A Multi-Channel THz and Infrared Spectrometer for Femtosecond Electron Bunch Diagnostics by Single-Shot Spectroscopy of Coherent Radiation. *Nucl. Instrum. Meth.*, A665:40–47, 2011.

[17] M. D. Litos, M. R. Bionta, V. A. Dolgashev, R. J. England, D. Fritz, S. Gilevich, Ph. Hering, and M. J. Hogan. Evaluation of Temporal Diagnostic Techniques for Two-Bunch FACET Beam. *Conf. Proc.*, C110328:568–570, 2011.

[18] S. J. Smith and E. M. Purcell. Visible light from localized surface charges moving across a grating. *Phys. Rev.*, 92:1069–1069, Nov 1953.

[19] G. Doucas, J. H. Mulvey, M. Omori, J. Walsh, and M. F. Kimmitt. First observation of smith-purcell radiation from relativistic electrons. *Phys. Rev. Lett.*, 69:1761–1764, Sep 1992.

[20] K. Ishi, Y. Shibata, T. Takahashi, S. Hasebe, M. Ikezawa, K. Takami, T. Matsuyama, K. Kobayashi, and Y. Fujita. Observation of coherent smith-purcell radiation from short-bunched electrons. *Phys. Rev. E*, 51:R5212–R5215, Jun 1995.

[21] K. Ishiguro and T. Tako. An Estimation of Smith-Purcell Effect as the Light Source in the Infra-red Region. *Optica Acta*, 8:25–31, 1961.

[22] G. Toraldo di Francia. On the theory of some Čerenkovian effects. *Il Nuovo Cimento*, 16:61–77, April 1960.

[23] D. V. Karlovets and A. P. Potylitsyn. Comparison of smith-purcell radiation models and criteria for their verification. *Phys. Rev. ST Accel. Beams*, 9:080701, Aug 2006.

[24] M.S. Malovytsia and N. Delerue. Comparison of the Smith-purcell Radiation Yield for Different Models . In *IPAC2016*, Proceedings of IPAC2016, page MOPMB004, Busan, South Korea, May 2016.

[25] D.V. Karlovets and A.P. Potylitsyn. Smith-purcell radiation in the ?pre-wave? zone. *JETP Letters*, 84(9):489–493, 2007.

[26] J. H. Brownell, J. Walsh, and G. Doucas. Spontaneous Smith-Purcell radiation described through induced surface currents. *Phys. Rev. E*, 57:1075–1080, Jan 1998.

[27] C.A. Ekdahl. High power microwave generator, June 24 1986. US Patent 4,596,967.

[28] J. M. Wachtel. Free-electron lasers using the smith-purcell effect. *Journal of Applied Physics*, 50(1):49–56, 1979.

[29] Levi Schächter and Amiram Ron. Smith-purcell free-electron laser. *Phys. Rev. A*, 40:876–896, Jul 1989.

[30] H. L. Andrews and C. A. Brau. Gain of a smith-purcell free-electron laser. *Phys. Rev. ST Accel. Beams*, 7:070701, Jul 2004.

[31] J. Gardelle, P. Modin, and J. T. Donohue. Start current and gain measurements for a smith-purcell free-electron laser. *Phys. Rev. Lett.*, 105:224801, Nov 2010.

[32] P Rullhusen, X Artru, and P Dhez. *Novel radiation sources using relativistic electrons: from infrared to x-rays*. Synchrotr Radiat. Techniques Appl. World Scientific, Singapore, 1998.

[33] C. Brau, C. Boulware, and H. Andrews. Smith-purcell free electron laser and method of operating same, March 23 2006. US Patent App. 11/172,429.

[34] D.C. Nguyen. Measuring short electron bunch lengths using coherent smith-purcell radiation, March 30 1999. US Patent 5,889,797.

[35] A. Doria, G.P. Gallerano, E. Giovenale, G. Messina, G. Doucas, M.F. Kimmitt, H.L. Andrews, and J.H. Brownell. Can coherent smith–purcell radiation be used to determine the shape of an electron bunch? *Nuclear Instruments and Methods in Physics Research Section A: Accelerators, Spectrometers, Detectors and Associated Equipment*, 483(1):263 – 267, 2002. Proceedings of the 23rd International Free Electron Laser Confere nce and 8th FEL Users Workshop.

[36] G. Doucas, M. F. Kimmitt, A. Doria, G. P. Gallerano, E. Giovenale, G. Messina, H. L. Andrews, and J. H. Brownell. Determination of longitudinal bunch shape by means of coherent smith-purcell radiation. *Phys. Rev. ST Accel. Beams*, 5:072802, Jul 2002.

[37] G. Doucas et al. Longitudinal electron bunch profile diagnostics at 45-MeV using coherent Smith-Purcell radiation. *Phys. Rev. ST Accel. Beams*, 9:092801, 2006.

[38] V. et al. Blackmore. First measurements of the longitudinal bunch profile of a 28.5 GeV beam using coherent Smith-Purcell radiation. *Phys. Rev. ST Accel. Beams*, 12:032803, Mar 2009.

[39] Nicolas Delerue, George Doucas, Ewen Maclean, and Armin Reichold. Longitudinal bunch profile diagnostics in the 50fs range using coherent Smith-Purcell radiation. 2009.

[40] R Bartolini, C Clarke, N Delerue, G Doucas, and A Reichold. Electron bunch profile reconstruction in the few fs regime using coherent Smith-Purcell radiation. *Journal of Instrumentation*, 7(01):P01009, 2012.

[41] H.L. Andrews, F. Bakkali Taheri, J. Barros, R. Bartolini, L. Cassinari, C. Clarke, S. Le Corre, N. Delerue, G. Doucas, N. Fuster-Martinez, I. Konoplev, M. Labat, C. Perry, A. Reichold, S. Stevenson, and M. Vieille Grosjean. Longitudinal profile monitors using coherent Smith-Purcell radiation. In Jens Osterhoff Arnd E. Specka Ralph Assmann, Massimo Ferrario, editor, *1st European Advanced Accelerator Concepts Workshop (EAAC2013)*, volume 740, pages 212–215, La Biodola, Italy, June 2013. Elsevier.

[42] L. Andrews, H. F. Bakkali Taheri, J. Barros, R. Bartolini, V. Bharadwaj, C. Clarke, N. Delerue, G. Doucas, N. Fuster-Martinez, M. Vieille-Grosjean, V. Konoplev, I. M. Labat, S. Le Corre, C. Perry, A. Reichold, and S. Stevenson. Reconstruction of the time profile of 20.35 gev, subpicosecond long electron bunches by means of coherent smith-purcell radiation. *Phys. Rev. ST Accel. Beams*, 17:052802, May 2014.

[43] J H Brownell, G Doucas, M F Kimmitt, J H Mulvey, M Omori, and J E Walsh. The angular distribution of the power produced by smith-purcell radiation. *Journal of Physics D: Applied Physics*, 30(17):2478, 1997.

[44] http://www.tau.ac.il/ phchlab/. Spectrum of the hydrogen atom.

[45] J. H. Brownell and G. Doucas. Role of the grating profile in Smith-Purcell radiation at high energies. *Phys. Rev. ST Accel. Beams*, 8:091301, 2005.

[46] C. A. J. Palmer and Loewen E. *Diffraction grating handbook*. Newport Corporation, 2005.

[47] D.A. Zhuravlev. E. g. loewen and e. popov diffraction gratings and their applications (marcel dekker, new york, 1997). *Optics and Spectroscopy*, 88(1):143–144, 2000.